

# EXPERIMENTAL INVESTIGATION OF UNSTEADY TRANSITION ON A PITCHING ROTOR BLADE AIRFOIL

K. Richter<sup>1</sup>, S. Koch<sup>2</sup>, A.D. Gardner<sup>3</sup>, H. Mai<sup>4</sup>, A. Klein<sup>5</sup> and C.-H. Rohardt<sup>6</sup>

<sup>1</sup>Institute of Aerodynamics and Flow Technology, DLR, Germany (kai.richter@dlr.de)

<sup>2,3,6</sup>Institute of Aerodynamics and Flow Technology, DLR, Germany

<sup>4</sup>Institute of Aeroelasticity, DLR, Germany

<sup>5</sup>Institute of Aerodynamics and Gas Dynamics, University Stuttgart, Germany

## Abstract

The unsteady flow around the pitching helicopter main rotor blade airfoil EDI-M109 was experimentally investigated at conditions similar to those existing on a retreating rotor blade in forward flight. High speed pressure measurements and hot film anemometry were used to investigate the unsteady transition characteristics of the airfoil. Results are presented for dynamic test points with attached flow, light dynamic stall and deep dynamic stall at  $M = 0.3$  and  $Re = 1.8 \times 10^6$ . The results include the discussion of the periodicity of the hot film signals for different flow states. The transition process of the pitching airfoil is analysed and the significance of the intermittent region is described. A time delay between the transition and the model motion is discussed and a linear relationship between the transition position and the time is observed. The influences of the pitching amplitude on the transition characteristics are discussed and the flow separation initiating dynamic stall is analysed.

## 1. INTRODUCTION

Design strategies for helicopter main rotor blade airfoils have classically used the steady performance for static polars. Recent design methodologies also take the dynamic performance of the oscillating airfoil into account in order to increase its performance in the rotor environment and to reduce negative effects such as dynamic stall [1]. In addition to the conventional steady aerodynamic parameters, unsteady flow characteristics, such as unsteady laminar/turbulent boundary layer transition, dynamic flow separation and reattachment are of special interest. The unsteady transition is of particular interest, as it affects both the performance for attached flow and the dynamic stall characteristics.

Modern industrial rotor blade airfoils are designed to have as much laminar flow as possible, since laminarisation is the most effective means for drag reduction in attached flows. As reliable CFD transition prediction methods currently only exist for steady airfoil flows, transition is considered in the design process only for steady conditions. The development of unsteady transition prediction tools

has begun but is still in its early stages. Currently, the only method of obtaining information about the unsteady transition behaviour is measurement in wind tunnel experiments. This data is also needed for the validation of the predictive tools.

The measurement of unsteady transition on a pitching airfoil or a rotating blade is complicated and expensive. Due to this, measurements on a full rotor do not exist in the literature. Measurements on pitching airfoils exist but are rare. Some work has been published for symmetric NACA airfoils for incompressible flows at Mach numbers of  $M \leq 0.1$  and low Reynolds numbers of  $Re \leq 3 \times 10^6$  [2] - [5]. For the compressible flow around non-symmetric rotor blade airfoils at conditions relevant for the retreating or advancing blade, only a small dataset is available in the literature by Lorber & Carta [6]. This is currently a problem for the calibration of CFD codes, since the effect of transition on the performance prediction is of the same order of magnitude as the effect of turbulence modelling [7].

The unsteady flow around the pitching main rotor blade airfoil EDI-M109 [8] was experimentally investigated in a cooperation between the national funded German research project INROS and the

joint DLR/ONERA project SIMCOS. Unsteady transition was measured by using hot film sensors for flow conditions relevant for retreating blade of a helicopter in forward flight.

## 2. EXPERIMENTAL ARRANGEMENT

A two-dimensional model of the rotor blade airfoil EDI-M109 was used. The carbon-fibre composite model had a chord of  $c = 300\text{mm}$ , a span of  $b = 997\text{mm}$ , and a maximum thickness of  $t_{\text{max}}/c = 9\%$ . The model was mounted horizontally in the  $1\text{m} \times 1\text{m}$  adaptive-wall test section of the Transonic Wind Tunnel Göttingen (DNW-TWG) and was driven with pitch-oscillations from drive shafts through the sidewalls attached at the quarter-chord position, shown in Fig. 1. The adaptive test section has flexible top and bottom walls which were statically adapted at the mean angle of attack of the model to minimise the interference velocities at the wall. Hydraulic motors, located outside the test section, drove the model from both sides. The model was fitted with 48 Kulite unsteady pressure sensors in one section, situated to guarantee a maximum discretization error of 1% in the lift and pitching moment coefficients evaluated from the pressure taps.

The model was additionally equipped with 40 customized Senflex<sup>®</sup> hot film sensors distributed on two Kapton sheets on the upper and lower side of the model. The sensor array layout, the arrangement of the sheets on the model and the electrical integration were designed to minimize disturbance of the measurements and of the airfoil flow in general. The sensors were placed on a line with an inclination of  $15^\circ$  to the main flow direction to prevent the passage of a sensor's wake over other sensors. The upper-side sheet was wrapped around the model leading edge and contained 24 sensors between  $x/c = 70\%$  on the model upper side and  $x/c = 5\%$  on the model lower side. The sensors had a standard spacing of  $\Delta x/c = 5\%$  and a reduced spacing of  $\Delta x/c = 1\%$  around the leading edge. The lower-side sheet was completely attached to the lower model side and contained 16 standard-spaced sensors between  $x/c = 20\%$  and  $x/c = 95\%$ . The sheets were glued onto the model in specially-prepared recesses, so that no additional thickness

was added to the model. The electrical wiring was installed inside of the model. Fig. 2 shows the distribution of the hot film sensors in the model cross section. The sensors are numbered T1 to T40. For simplicity, the sensor position will be used with positive and negative value to indicate sensors on the upper side and lower side. The layouts of the hot film arrays are depicted in Fig. 3.



Fig. 1: The EDI-M109 airfoil model with hot film sensors installed in the DNW-TWG wind tunnel

The hot film sensor arrays consisted of nickel sensor elements and copper leads. The sensor elements had a length of  $1.4\text{mm}$ , a width of  $0.1\text{mm}$  and a height of  $0.2\mu\text{m}$ . The nominal cold resistance was around  $6\Omega/\text{mm}$  resulting in a resistance of the sensor element of approx.  $9\text{--}10\Omega$ . The copper leads had a width of  $3.05\text{mm}$ , height of  $4.2\mu\text{m}$  and varying lengths due to the layout of the array. The nominal cold resistance of the leads was around  $0.004\Omega/\text{mm}$ , leading to a maximum resistance of the longest lead of approx.  $1.4\Omega$ . The resistance ratio of sensor elements to leads was therefore higher than 7 for the entire array.

The hot film sensors were operated in constant-temperature mode. No calibration was performed since a calibration for unsteady base flows is very complicated and the objective of this experiment was to investigate the qualitative time-dependent behaviour of the boundary layer shear stress characteristics but not the quantitative measurement of the shear stress itself. Data was sampled at a rate

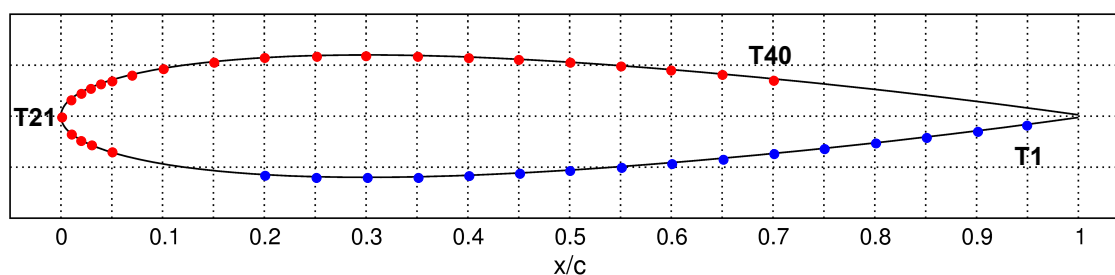


Fig. 2: Hot film sensor distribution in the model cross section (mapped to NACA0012 airfoil geometry)

of approximately  $f = 120\text{kHz}$  and synchronized with the pressure measurements which were performed with 1024 samples per model pitching period. Both the hot film and the pressure data were recorded for 160 periods.

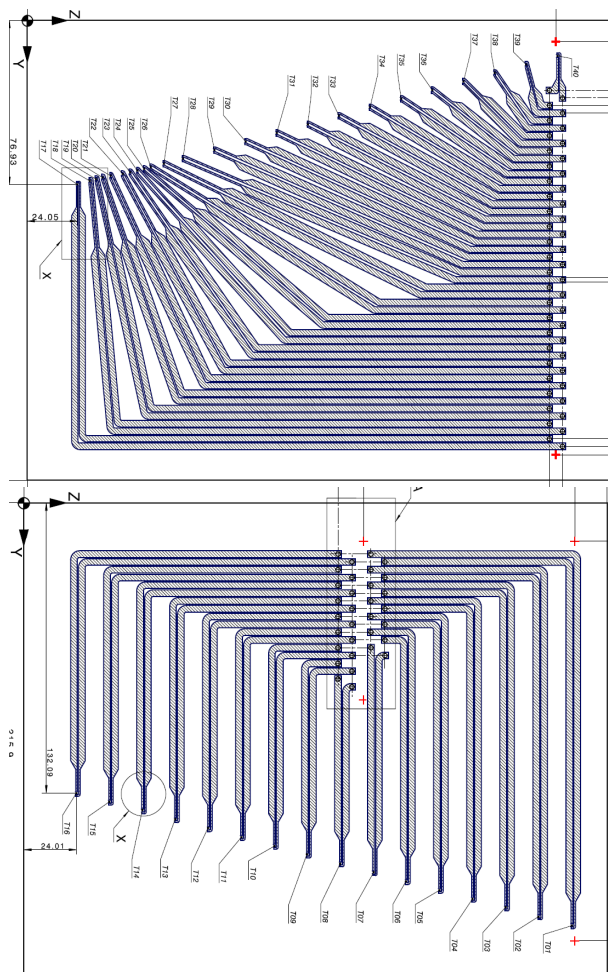


Fig. 3: Layouts of the hot film sensor arrays for model upper side (top) and lower side (bottom)

Measurements were conducted for dynamic test points with conditions similar to those existing on the retreating main rotor blade in forward flight. Sinusoidal pitching motion around different mean angles of attack  $\alpha_0 = [8^\circ, 10^\circ, 12^\circ]$  and different amplitudes  $\alpha_1 = [4^\circ, 5^\circ, 6^\circ, 7^\circ]$  was performed at a constant frequency of  $f = 6.6\text{Hz}$ . Mach numbers of  $M = [0.3, 0.4, 0.5]$  were investigated at a constant Reynolds-number to Mach-number ratio of  $Re/M = 6 \times 10^6$ . This publication concentrates on the results obtained for  $M = 0.3$  and  $Re = 1.8 \times 10^6$ . The data covers test points with attached flow over the entire cycle, light dynamic stall and deep dynamic stall cases.

### 3. DATA ANALYSIS

A hot film sensor operated in constant-temperature mode measures the electrical voltage needed to compensate the heat transfer from the heated sensor into the cooling air flow. Using the Reynolds analogy, the heat transfer through the hot film is related to the local wall shear stress. The hot film sensors can thus be used to detect flow phenomena that are associated with a change in wall shear stress. This is the case for boundary layer transition, flow reversal and flow separation.

The analysis of the hot film sensor data was conducted for the voltage signals of the individual sensors. In contrast to hot film anemometry in steady base flows, where automatic analysis tools are able to detect boundary layer transition from the mean value, standard deviation and skewness of the signal, this is not possible for the signals measured in this experiment on the pitching airfoil model. In steady flows each sensor signal reflects only a single state of the boundary layer at the position of the sensor. For the unsteady flow around a pitching airfoil, the boundary layer state at a sensor varies with time and can contain all phases of laminar/turbulent transition, relaminarisation, separation and also vortex shedding. Each sensor signal has to be analysed by hand, making the analysis of pitching airfoil hot film data very expensive.

#### 3.1. Stagnation Point Movement

For a pitching airfoil, the variation of the angle of attack leads to a movement of the stagnation point along the airfoil contour. The stagnation point divides the airfoil flow into upper side flow and lower side flow, and is the starting point for the upper and lower side boundary layers. A variation in the stagnation point location thus leads to a variation of the boundary layer characteristics at a fixed sensor position. Therefore, all sensor signals exhibit a basic wavy behaviour for attached flow cases, regardless of the type of boundary layer, as can be seen in time-dependent voltage signals in Fig. 4.

For sensor T21 at  $x/c = 0\%$ , the stagnation point is always located on the lower model side. Therefore, the sensor is always in the upper side airfoil flow. Increasing the angle of attack in the periodic pitching motion, causes a downstream movement of the stagnation point and increases the length and the thickness of the boundary layer at the sensor position. The wall shear stresses increase, and this leads to a rise in the heat transfer reflected by the increasing voltage of the hot film with the model incidence. Similarly, a decreasing angle of attack causes a corresponding decrease in the voltage, causing the wavy behaviour of the sensor signals over a pitching cycle. Whereas the flow over T21 is fully laminar, the fully turbulent signal of T32 at

$x/c = 30\%$  qualitatively shows the same behaviour but with a reduced waviness. This reduction is caused since the sensor is far from the stagnation point and the relative change in the boundary layer properties is reduced.

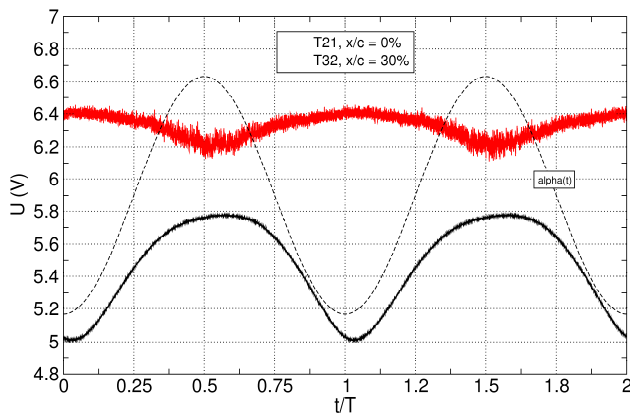


Fig. 4: Time-dependent voltage output for laminar and turbulent signals

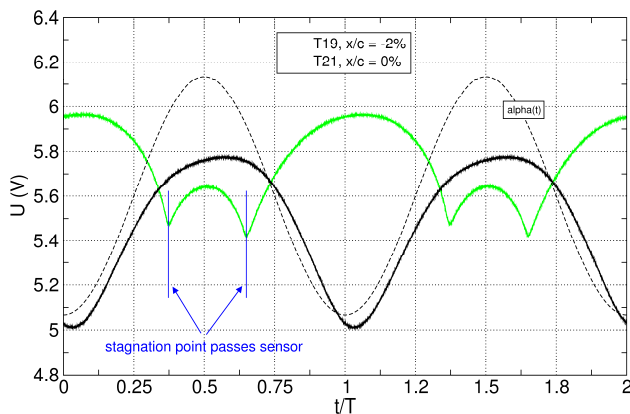


Fig. 5: Time-dependent voltage output for laminar signals with stagnation point movement over the sensor

When sensors are placed in the region of the stagnation point movement, this movement can be detected. Lee et al [3] identified the passage of the stagnation point over a sensor with a local minimum in the sensor voltage. This can also be seen in the current measurements. The much higher temporal resolution of the data, however, allows the stagnation point passage to be seen as a folding of the signal, as shown in Fig. 5 for sensor T19 located at  $x/c = -2\%$ . In the period of time between  $t/T = 0.373$  and  $t/T = 0.649$ , the signals of T19 and T21 follow the same trend, indicating that they are in the same boundary layer, i.e. they have the same flow direction. In the rest of the period, the signals exhibit opposite trends, indicating that they now belong to opposite boundary layers. The flow over the sensors has the opposite direction and the stagnation point is located between the sensors. The instances of time  $t_1$  and  $t_2$ , at which the signal folds, are the moments when the stagnation point is

exactly above the sensor. This definition is used for the discussion of the stagnation point movement later in the paper. When the signal is manually inverted in time and voltage, it can be demonstrated that it completes the original T19 signal, and two artificial signals appear which are not folded.

### 3.2. Boundary Layer Transition

Superimposed over the basic wavy behaviour, the hot film sensor signals allow for the determination of laminar and turbulent flow states. Fig. 6 shows the time-dependent voltage signal of sensor T26 located at  $x/c = 5\%$  and the standard deviation computed over all periods. This typical signal can be divided into four regions: laminar flow, intermittency from laminar to turbulent, turbulent flow, intermittency from turbulent to laminar (and again laminar flow).

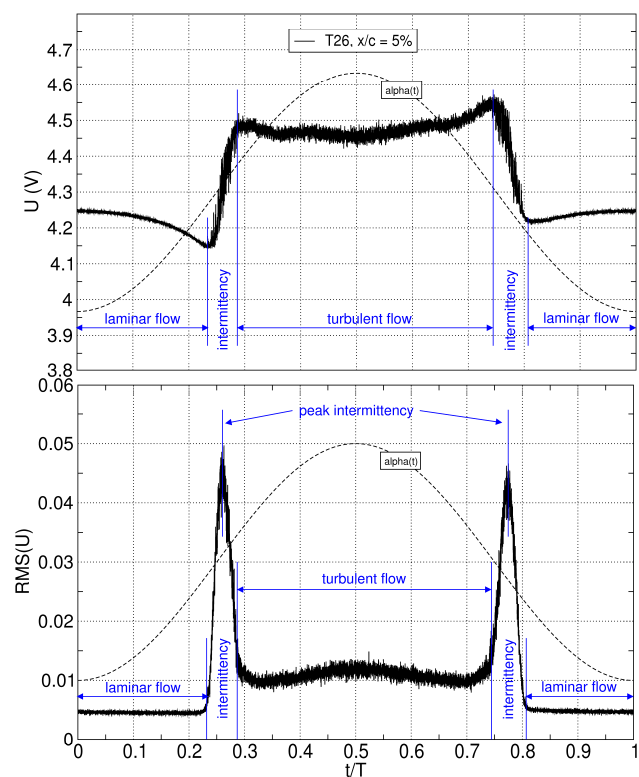


Fig. 6: Time-dependent voltage (top) and standard deviation (bottom) for the sensor T26 at  $x/c = 5\%$

Laminar flow is characterised by a low mean voltage and a very low standard deviation, as both the wall shear stresses and the fluctuations are small in a laminar boundary layer. At  $t/T = 0.231$  the end of full laminarity is reached and intermittency begins. As known from transition measurements in steady base flows [5], the signal is now mainly laminar but progressively reveals turbulent peaks. The standard deviation rises and the mean voltage increases as the wall shear stress grows. Peak intermittency is reached with the maximum in RMS at  $t/T = 0.260$ . The boundary layer here is exactly between the two

states. Further on, the standard deviation decreases again since the boundary layer becomes increasingly turbulent. Correspondingly, the shear stresses increase further as indicated by the rising mean voltage. At  $t/T = 0.287$ , the fully turbulent levels are reached with a roughly constant RMS and mean voltage. Both are on higher levels than for laminar flow since both the fluctuations and the wall shear stresses are higher in a turbulent boundary layer than in laminar flow. The end of the fully turbulent state is reached at  $t/T = 0.744$ , when the intermittent region begins with a rising RMS and a decreasing mean voltage. The signal is now mainly turbulent but progressively reveals laminar peaks. At  $t/T = 0.774$ , peak intermittency is reached for the relaminarisation and at  $t/T = 0.807$  the fully laminar state is reached, defining the beginning of the laminar region.

The data measured with the EDI-M109 airfoil reveals significant intermittent regions for the test cases investigated. This requires a separate examination of the beginning, peak and end of intermittency. Therefore, no general 'transition location' will be defined in this work. Instead, it will be distinguished between 'fully laminar', 'fully turbulent' and 'peak intermittency' to provide additional insight into the characteristics of the intermittent boundary layer state on a pitching airfoil. This finding differs to the results published by Schreck et al [2], Lee et al [3][5], and Chandrasekhara & Wilder [4] for different airfoils, flow speeds and Reynolds numbers. In their work, only a universal 'transition location' or 'transition onset location' was used. It is currently not clear whether the intermittent region was much smaller in their cases or whether the lower temporal resolution did not permit a more detailed determination.

### 3.3. Flow Separation

As flow separation causes a change in the local wall shear stresses, hot film sensors can also be used to detect separation. This was previously shown by Kiedaisch & Acharya [9] and Schreck et al [10] for flow separation at the position of the sensor. This direct detection of separation is also possible with the data measured in this work, and separation is clearer due to the very high temporal resolution of the data. Fig. 7 shows a laminar/turbulent signal of sensor T26 at  $x/c = 5\%$  with separation in the turbulent flow regime. Since the wall shear stress significantly reduces and fluctuations significantly increase in separated flow, separation can be seen by a drop in the voltage and a strong increase in the standard deviation. Separation takes place at  $t/T = 0.471$ . The continuous degradation of the voltage and the slow rise of the standard deviation prior to separation onset, indicates that the separation is caused by the weakening of the turbulent boundary layer. The moment of separation

is reached when the sudden jump to a high RMS level takes place. During separation, sensor voltage is low and standard deviation is much higher than for attached turbulent flow. Reattachment occurs at  $t/T = 0.613$  and can be detected more clearly in the standard deviation plot than in the voltage plot. The sudden orderliness of the flow causes a sharp drop in standard deviation, whereas it causes only a relatively small kink in the voltage output. In the present example, the turbulent RMS level is reached after reattachment and not the laminar level, indicating that turbulent reattachment has taken place.

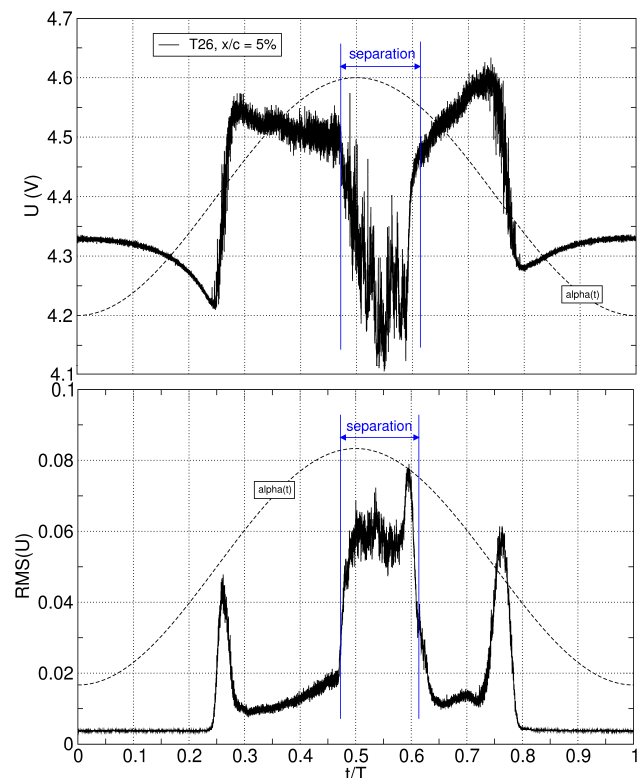


Fig. 7: Time-dependent voltage (top) and standard deviation (bottom) for sensor T26 at  $x/c = 5\%$

In addition to the direct detection of flow separation, the data in this work also allows for an indirect detection of the occurrence of flow separation elsewhere on the airfoil. Since flow separation alters the circulation of the airfoil, a small shift of the stagnation point is caused when the airfoil flow separates. The stronger the separation and the higher the loss in circulation, the stronger the movement of the stagnation point. The indirect separation detection therefore uses the observations made in section 3.1. Fig. 8 shows the voltage signal of sensor T21 at  $x/c = 0\%$  and the corresponding lift curve. The sensor signal shows fully laminar flow with stagnation point movement over the sensor.

Between  $t/T = 0.49$  and  $t/T = 0.61$  the hot film signal shows a linear decrease to lower voltage which interrupts the general wavy form of the signals. This

indicates loss of circulation due to flow separation as the stagnation point is translated upstream when circulation is reduced. At the same time, the lift breakdown is visible in the lift curves shown. Since sensor T21 is located in the upper side flow, the upstream shift of the stagnation point causes a reduction of the length of the boundary layer and therefore a reduction in voltage. This behaviour is best visible from signals of sensors near the location of the stagnation point since the relative change of the boundary layer length is large here. A sensor located in the lower side flow could also be used for the detection but a shift of the voltage level to higher values would occur. The upstream movement of the stagnation point during separation then increases the length of the lower side boundary layer.

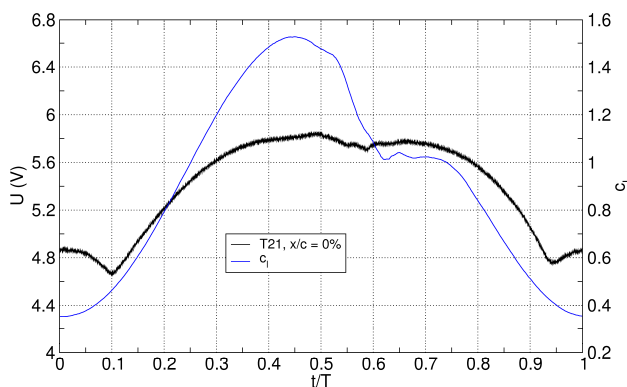


Fig. 8: Time-dependent lift curve (top) and voltage output (bottom) of sensor T21 at  $x/c = 0\%$

## 4. RESULTS AND DISCUSSION

Boundary layer transition, flow separation and stagnation point movement were investigated based on the hot film and pressure data measured on the pitching EDI-M109 rotor blade airfoil. Results will be presented for  $M = 0.3$  and  $Re = 1.8 \times 10^6$  relevant for the retreating rotor blade of a helicopter in forward flight.

### 4.1. Periodicity of the results

The hot film data was sampled with a frequency of  $f = 120\text{kHz}$  over 160 model pitching periods at an oscillation frequency of  $f = 6.6\text{Hz}$ . This resulted in approximately  $3 \times 10^6$  data points per sensor and test case, or roughly  $120 \times 10^6$  data points for the entire hot film array per test case measured. As no tools currently exist for the automatic analysis of hot film data of pitching airfoils, the manual analysis is very time consuming. The worst case would be the necessity to analyse the sensor outputs for every individual period when the data may be of insufficient periodicity.

In the present work, periodicity was therefore checked for purely laminar, transitional and purely

turbulent signals, and for signals with flow separation over the sensor. The analysis was performed by the comparison of mean voltage and standard deviation of individual periods with phase-averaged data. Phase-averaging was conducted for 159 periods for each of the 17920 data points in a cycle. For the individual periods, mean and standard deviation were computed in sliding windows of 200 data points with an overlap of 10 points. The validity of the comparison of different types of mean values is not in question. The comparison of the different types of standard deviation, however, is questionable as it compares the deviation within a period of time in a cycle with the cycle-by-cycle deviation at a point of the period. This has to be used with caution as it can lead to non valid comparisons, but it was found to be a good means to check the periodicity of flow phenomena that are associated with strong stochastic fluctuations.

Purely laminar and purely turbulent signals show good periodicity. Apart from a minor scatter of the absolute voltage values, the wave-form of the signals is unchanged and the temporal relation is not affected. The same holds for signals with stagnation point movement over the sensor. The instance of time when the stagnation point passes the sensor is reflected precisely in all periods, as shown in Fig. 9 by the mean voltage curves computed by window-averaging for every individual period (coloured curves) or computed cycle-to-cycle by phase-averaging (single black line).

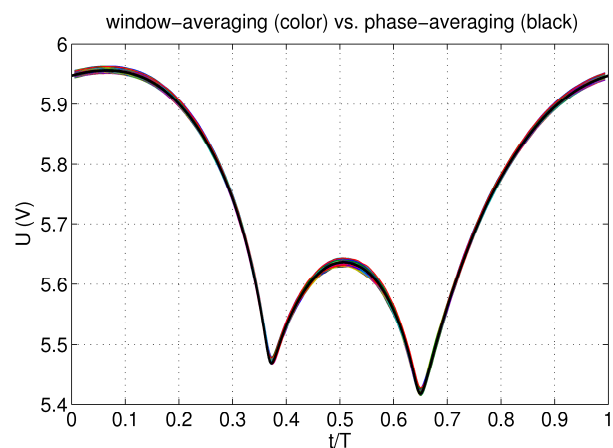


Fig. 9: Mean voltage of a laminar signal computed by window-averaging and phase-averaging

Transitional signals were also found to be periodic. Here, the analysis of both the mean and the standard deviations give meaningful results, shown in Fig. 10. As seen for fully laminar and turbulent flow, the scatter in the mean voltage of the transitional signal is also small and all important features of the sensor output exist in both types of analysis. The temporal scatter in the intermittent

region is approximately  $\Delta t/T = 0.005$ . When using the standard deviation for comparison, the same very small temporal scatter can be observed but large differences occur with respect to the absolute RMS values. However, both the qualitative characteristics of the RMS output and the quantitative temporal information are kept. The important information such as the beginning/end of the laminar/turbulent regimes and the peak intermittency are periodic.

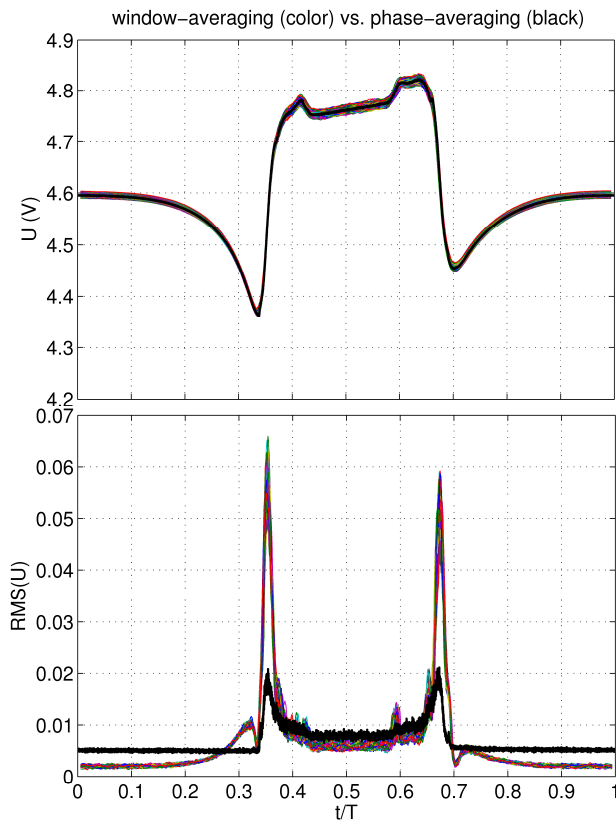


Fig. 10: Mean voltage (top) and standard deviation (bottom) of a transitional signal computed by window-averaging and phase-averaging

Hot film sensor signals with flow separation exhibit periodic and non periodic parts. Fig. 11 (top) shows the mean voltage outputs for a typical signal with turbulent separation and turbulent reattachment. Prior to separation, the signal is periodic. The temporal scatter in the laminar-turbulent intermittent region is as small as in the transitional cases without separation, compare Fig. 10. With the onset of separation the scatter starts to increase but the time of separation onset is still periodic. With progressing separation, the scatter becomes large and reaches its maximum when full separation is reached. The flow states at the sensor now exhibit large cycle-to-cycle variations and the onset of reattachment varies strongly. In this case, the latest reattachment is chosen as the end of separation for the further data analysis in this work. As relaminarisation occurs in this case only shortly after the reattachment, the

onset of relaminarisation is similarly affected. As a consequence, both the turbulent-laminar intermittency and the beginning of the fully laminar region show large cycle-to-cycle variations. In such cases, the phase-averaged output was chosen for analysis which provided the earliest end of the turbulent region and the latest beginning of fully laminar flow.

In cases in which the relaminarisation has a larger time lag to the reattachment, the flow is able to stabilise prior to the onset of relaminarisation. Hence, the cycle-to-cycle variations reduce significantly and reach almost the same level as prior to the separation, shown in Fig. 11 (bottom). Relaminarisation then happens again periodically with a temporal scatter only slightly larger than without separation.

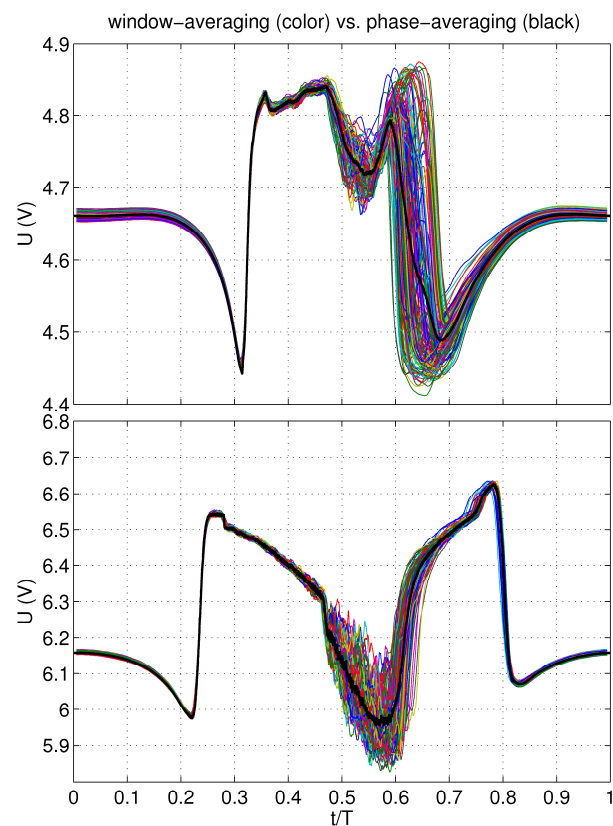


Fig. 11: Mean voltage of signals with separation computed by window-averaging and phase-averaging

## 4.2. Unsteady Transition

### 4.2.1. Test case with fully attached flow

The test case with mean angle of attack of  $\alpha_0 = 8^\circ$  and amplitude of  $\alpha_1 = 4^\circ$  was chosen for the initial analysis of unsteady transition on the pitching EDI-M109 airfoil. The test case has lift curves that are almost sinusoidal, indicating that no flow separation

occurs during the pitching cycle. Fig. 12 shows the upper side transition parameters and the lift coefficient as a function of time for two model motion periods. As discussed in section 3.2, the transition parameters are split into the end of fully laminar flow, the point of peak intermittency and the beginning of fully turbulent flow.

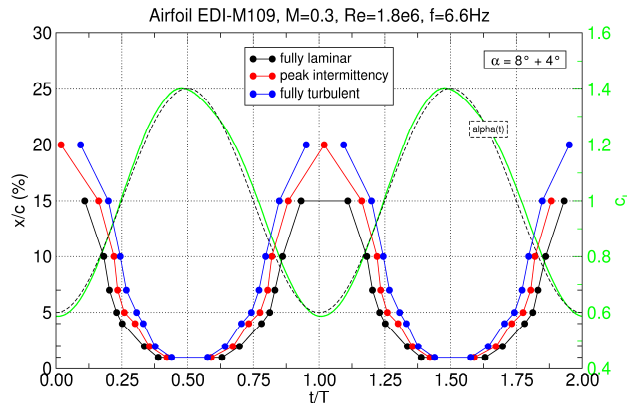


Fig. 12: Unsteady transition parameters and lift coefficient as a function of time for the test case with fully attached flow

The pitching EDI-M109 airfoil shows an unsteady movement of the upper side transition location with varying model angle of attack. As was expected, an upstream movement of the transition is observed during the upstroke and a downstream movement during the downstroke. This is in agreement with the results published by Lorber & Carta [6] and Lee & Gerontakos [5] for the other airfoils. For the modern EDI-M109, maximum laminar flow up to  $x/c < 20\%$  is reached around minimum angle of attack. With increasing angle, the end of the laminar region rapidly moves upstream and reduces its forward speed near the leading edge. The most upstream end of the laminar region was detected at the sensor at  $x/c = 1\%$ . The leading-edge sensor at  $x/c = 0\%$  was laminar for the entire cycle. The downstroke behaviour of the end of laminarity was found to be completely symmetric to its behaviour during the upstroke. However, a small time delay was observed for the entire transition movement compared to the model motion. Maximum laminarity is reached  $\Delta t/T \approx 0.02$  after the minimum angle of attack is passed.

The transition behaviour of the beginning of the fully turbulent region is basically similar to the behaviour of the laminar end. However, a significant spatial distance exists which forms the intermittent region where the flow is changing from laminar to turbulent. The smallest turbulent region extends to at least  $x/c = 25\%$  since the sensor at this position was fully turbulent for the entire period. The largest portion of turbulent flow extends up to  $x/c = 1\%$  when the model is around maximum angle of attack. The streamwise extent of the intermittent region is

largest at minimum angle of attack and reaches approximately  $\Delta x/c = 8\%$ . It reduces during the upstroke and reaches values smaller than  $\Delta x/c = 1\%$  at maximum angle of attack when transition takes place at the leading edge. The time period in which intermittency happens was observed as  $\Delta t/T = 0.09$  at  $x/c = 15\%$  and  $\Delta t/T = 0.05$  at  $x/c = 1\%$ . Considering both upstroke and downstroke, means that the flow over these sensors is 10% to 20% of the cycle in an intermittent state.

The peak intermittency takes place approximately at the midpoint between laminar end and turbulent beginning for all instances. Downstroke and upstroke movements of peak intermittency and of the beginning of the turbulent region are again symmetric and have the same time delay of  $\Delta t/T \approx 0.02$  compared to the model motion, as was observed for the movement of the end of laminarity.

When plotting the transition parameters as a function of the angle of attack in Fig. 13, the large hysteresis between upstroke and downstroke becomes visible. At a constant streamwise location, transition occurs at higher angles of attack during upstroke than relaminarisation takes place during downstroke. The pitching motion therefore causes the enhancement of laminarity during upstroke and a suppression during downstroke. The hysteresis is largest at the most downstream position and reduces towards the leading edge. Concentrating only on one of the transition parameters, e.g. the end of laminarity, a phase difference of  $\Delta\alpha \approx 1^\circ$  exists at  $x/c = 10\%$  which reduces to  $\Delta\alpha \approx 0.4^\circ$  at  $x/c = 1\%$ . For constant angle of attack at  $\alpha \approx 6.4^\circ$  the hysteresis results in  $\Delta x/c = 5\%$  ( $x/c = 15\%$  instead of  $x/c = 10\%$ ) more laminar flow on the upstroke than on the downstroke.

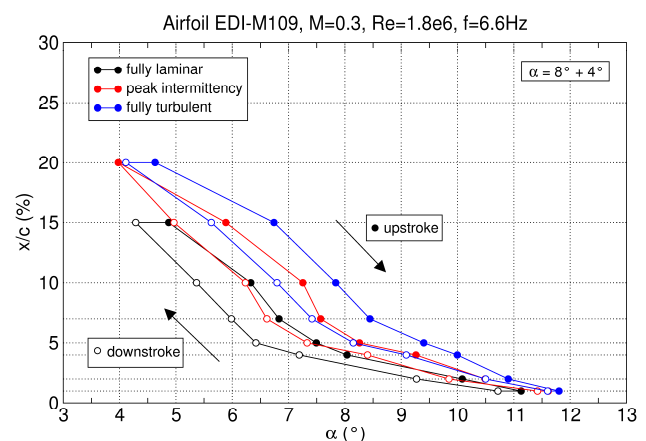


Fig. 13: Unsteady transition parameters as a function of angle of attack for the test case with fully attached flow

When looking at the angle-of-attack range of the intermittent flow region, it becomes clear that this undetermined boundary layer state has to be

respected in the development of future unsteady transition prediction tools. For the test case with pitching motion with  $4^\circ$  amplitude, the flow at  $x/c = 10\%$  on the model upper side is in an intermittent state for  $\Delta\alpha \approx 1.5^\circ$  during upstroke and  $\Delta\alpha \approx 1.4^\circ$  during downstroke. Up to now, most transition prediction tools try to avoid intermittent flow and aim for an instantaneous change of the boundary layer state. The data measured in this work indicates clearly, however, that intermittency is an important part of unsteady transition.

#### 4.2.2. Test case with dynamic stall

The unsteady transition behaviour of the EDI-M109 was also analysed for cases with dynamic stall. The test case with a mean angle of attack of  $\alpha_0 = 8^\circ$  and an amplitude of  $\alpha_1 = 6^\circ$  was chosen as an example for the detailed presentation. Fig. 14 shows the upper side transition parameters and the lift curve as functions of time for two model motion periods.

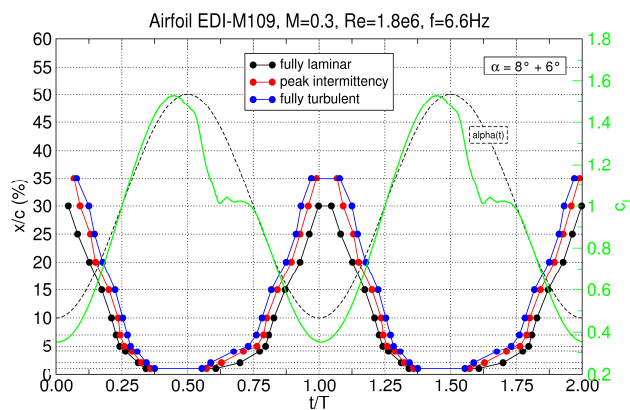


Fig. 14: Unsteady transition parameters and lift coefficient as a function of time for the test case with dynamic stall

In general, a similar transition movement occurs as for the attached flow case. Transition moves upstream with increasing angle of attack and downstream with decreasing model incidence. Since the minimum angle of attack is  $\Delta\alpha = 2^\circ$  lower than in the attached flow case, the maximum laminar length is significantly extended in the dynamic stall case. Around minimum angle of attack, maximum laminar flow exists up to  $x/c < 35\%$  and the latest beginning of the fully turbulent regime is shifted to at least  $x/c \leq 40\%$ . Around maximum angle of attack, transition takes place at the leading edge just as for the attached flow case, and the largest portion of turbulent flow extends again up to  $x/c = 1\%$ . The leading edge sensor at  $x/c = 0\%$  is again always laminar. The streamwise extent of the intermittent region is largest at minimum angle of attack, now reaching approximately  $\Delta x/c = 10\%$ , and reducing during the upstroke to values smaller than  $\Delta x/c = 1\%$  at maximum angle of attack. Although the spatial

length of the intermittent region increases compared to the attached flow case, it reduces its temporal length. The time period in which intermittency happens was observed as  $\Delta t/T = 0.05$  at  $x/c = 15\%$  and  $\Delta t/T = 0.03$  at  $x/c = 1\%$ . This contrast appears since the velocity of the transition movement is higher than before. Furthermore, a linear relationship develops for the transition parameters as a function of time, for positions downstream of  $x/c = 7\%$ . This linear relation does not exist for the case with reduced amplitude.

Although the transition behaviour of this case shows the same time delay  $\Delta t/T \approx 0.02$  to the model motion as in the attached flow case, the transition behaviour is no longer symmetric for upstroke and downstroke. Since flow separation occurs at the beginning of the downstroke, the circulation of the airfoil is changed and the transition movement is delayed compared to upstroke.

The similarities between the temporal transition behaviour of the dynamic stall case and the attached flow case also persist in the angular transition behaviour shown in Fig. 15. In general, the same basic trends occur. A significant hysteresis exists that is largest at the most downstream position and again reduces towards the leading edge. The hysteresis is even larger than before, now showing a phase difference for the end of laminarity at  $x/c = 10\%$  of  $\Delta\alpha \approx 1.3^\circ$  between upstroke and downstroke. For constant angle of attack at  $\alpha \approx 6.4^\circ$  the hysteresis results in  $\Delta x/c = 5.7\%$  more laminar flow on the upstroke than on the downstroke. In addition to the enlargement of the upstroke/downstroke hysteresis, it was found that the size of the intermittent region increases. At  $x/c = 15\%$ , the flow on the model upper side is in an intermittent state for  $\Delta\alpha \approx 1.8^\circ$  during the upstroke and  $\Delta\alpha \approx 1.7^\circ$  during the downstroke.

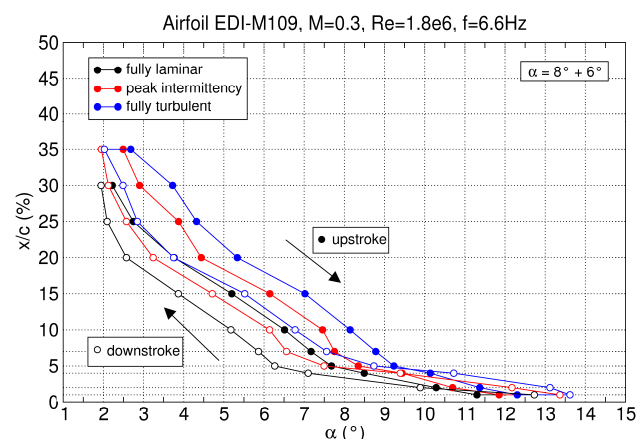


Fig. 15: Unsteady transition parameters as a function of angle of attack for the test case with dynamic stall

### 4.3. Influence of amplitude

The influence of the pitching amplitude on the unsteady transition behaviour, the separation and reattachment characteristics, and the stagnation point movement was investigated for four amplitudes  $a_1 = [4^\circ, 5^\circ, 6^\circ, 7^\circ]$  at constant mean angle of attack of  $a_0 = 8^\circ$ . The test cases include conditions without flow separation, with light dynamic stall and with deep dynamic stall.

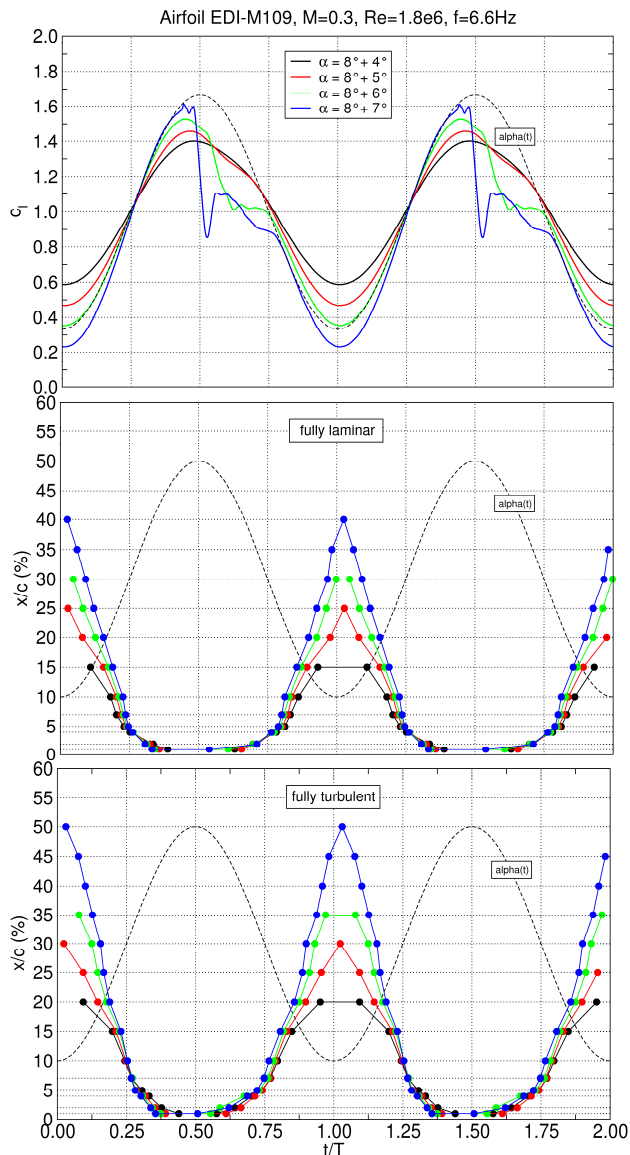


Fig. 16: Unsteady lift coefficients (top) and transition parameters (middle, bottom) as a function of time for the variation of the pitching amplitude

#### 4.3.1. Unsteady Transition

The largest influence of the pitching amplitude on the unsteady transition behaviour can be seen in the downstream extension of the transition location at low angles of attack. Fig. 16 shows the time-dependent lift coefficients and transition parameters

as a function of the amplitude. For the smallest amplitude  $\alpha_1 = 4^\circ$ , the maximum laminar length is  $x/c < 20\%$ , whereas  $x/c = 40\%$  is reached for the largest amplitude  $\alpha_1 = 7^\circ$ . The same behaviour is found for the location of the beginning of fully turbulent flow, which changes from  $x/c < 25\%$  to  $x/c = 50\%$ . All transition curves cross in the region of  $x/c = 5 - 7\%$ , in the moment the test cases have approximately the same lift coefficient. Downstream of this crossing point, a linear relationship between the transition parameters and the time develops. Therefore, the speed of the transition movement increases with increasing amplitude. Upstream of this crossing point, the influence of the amplitude is smaller and a constant most upstream transition position of  $x/c = 1\%$  is reached independent of the amplitude. During the upstroke hardly any influence was detected and all test cases have a very similar transition movement near maximum angle of attack. During the downstroke, the increasing amplitude leads to an earlier but slower downstream movement of the transition caused by the changes in circulation due to flow separation.

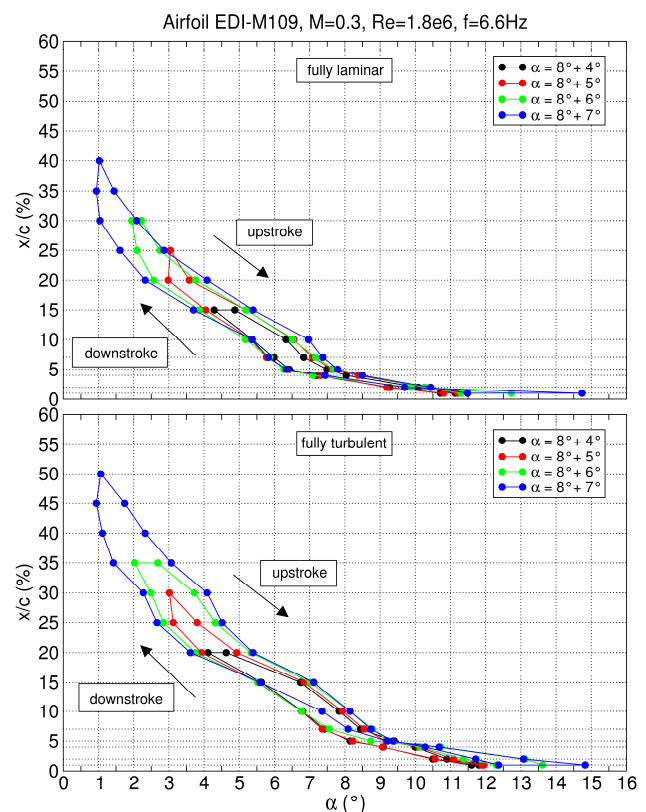


Fig. 17: Unsteady transition parameters as a function of angle of attack for the variation of the pitching amplitude

When plotting the transition parameters as a function of the angle of attack, shown in Fig. 17, it becomes visible that the transition hysteresis increases with the amplitude. The maximum transition location is shifted downstream, as seen

before, and the phase difference between upstroke and downstroke becomes larger. In addition, the hysteresis curves are nested, i.e. the hysteresis curve of a specific amplitude surrounds the curve for the next lower amplitude. This was found for all three transition parameters instigated. A different behaviour was only found for the dynamic stall test cases when stall occurs at very high angles of attack.

### 4.3.2. Separation

The influence of the amplitude on the unsteady separation behaviour was found in earlier separation and later reattachment with increasing amplitude. Fig. 18 shows the locations of separation and reattachment as a function of time for different amplitudes. For amplitudes  $\alpha_1 \leq 5^\circ$ , no separation was detected by the hot film sensors. There could have been some separation downstream of the maximum sensor position at  $x/c = 70\%$  for the test case with  $\alpha_1 = 5^\circ$  but this could not be measured. For higher amplitudes, separation and reattachment are indicated by the hot film sensor signals. As described in section 4.1, the hot film sensor signals are very stochastic during separated flow, and the moment the separation ends is not periodic. Therefore, the reattachment point given Fig. 18 reflects the latest reattachment detected in the signals.

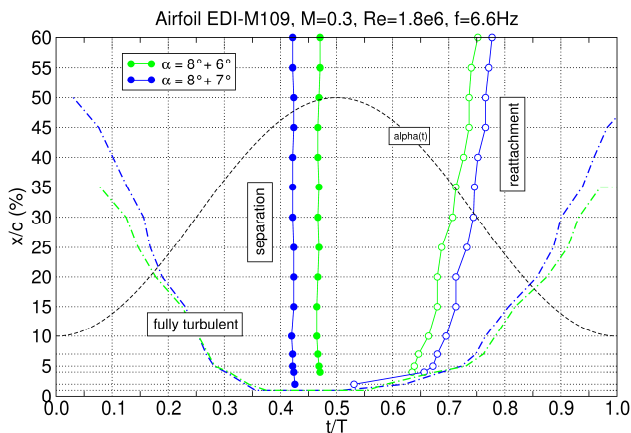


Fig. 18: Locations of separation and reattachment as a function of time for the variation of the pitching amplitude

For both amplitudes, the separation occurs as an abrupt detachment of the entire upper side airfoil flow from a position shortly downstream of the leading edge. With increasing amplitude, the separation location moves upstream from  $x/c = 4\%$  for  $\alpha_1 = 5^\circ$  to  $x/c = 2\%$  for  $\alpha_1 = 6^\circ$ . The comparison with the lines of the beginning of fully turbulent flow in Fig. 18 shows that turbulent separation occurs in both cases. Although there is a significant time difference between both instances of separation, the

stall angles of attack of both cases are close to each other:  $\alpha(t_1) = 13.90^\circ$  for  $\alpha_1 = 5^\circ$  and  $\alpha(t_2) = 14.15^\circ$  for  $\alpha_1 = 6^\circ$ . Turbulent reattachment happens from the leading edge with the reattachment point slowly progressing towards the trailing edge of the airfoil. As separation occurs earlier and reattachment happens later for higher amplitudes, the separated portion of the cycle increases with the amplitude.

No laminar separation was detected by the hot film sensors for the test cases investigated in this work, indicating that a laminar separation bubble is not involved in the dynamic stall process on the EDI-M109 airfoil at  $M = 0.3$  and the high Reynolds number of  $Re = 1.8 \times 10^6$ .

### 4.3.3. Stagnation Point Movement

The influence of the amplitude on the stagnation point movement is seen in an enhancement of the movement with increasing amplitude, shown in Fig. 19 by the stagnation point location plotted for the different test cases as a function of time. In the test cases investigated, the movement could be detected on sensors T18 to T21 from  $x/c = -3\%$  to  $x/c = 0\%$ . The stagnation point moves downstream during the upstroke, whereas it moves upstream during the downstroke. This behaviour is well known [3] and was expected. Only a small hysteresis exists for the test cases without stall. For test cases with dynamic stall, however, a large hysteresis was found with a significant deviation of the stagnation point location at high angles of attack. For attached flow at angles of attack of  $\alpha \approx 13^\circ$  and lower (compare section 4.3.2) the locations fit well into the smooth trends. At angles above  $\alpha = 13.9^\circ$ , abrupt separation occurs and the airfoil circulation is changed nearly instantaneously. Circulation reduces and the stagnation point is shifted upstream.

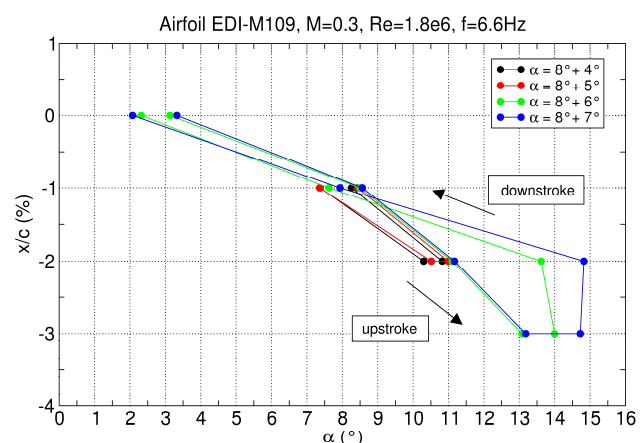


Fig. 19: Stagnation point movement as a function of angle of attack for the variation of the pitching amplitude

The spatial resolution of the measured stagnation point movement was found to be too coarse for

more detailed investigations. However, the present stagnation point location data is nevertheless valuable for the CFD code validation of dynamic stall simulations.

## 5. CONCLUSIONS

The unsteady flow around the pitching helicopter main rotor blade airfoil EDI-M109 was experimentally investigated at conditions similar to those existing on a retreating main rotor blade in forward flight. High speed pressure measurements and hot film anemometry were used to investigate the unsteady transition characteristics of the airfoil. Results were presented for dynamic test points with attached flow, light dynamic stall and deep dynamic stall at  $M = 0.3$  and  $Re = 1.8 \times 10^6$ .

The periodicity of the hot film data was checked for different flow conditions at the sensor. For attached flow, periodicity could be shown for signals in fully laminar or turbulent flow as well as for signals with boundary layer transition. When separation occurs, the separation point remains periodic whereas the reattachment point varies strongly. Relaminarisation is affected when it happens shortly after reattachment.

Transition takes place on the EDI-M109 by the growth of instabilities within the intermittent region. No laminar separation bubble was found for the test cases investigated. The data revealed the significance of the intermittency, as the intermittent region has a streamwise extent of up to  $\Delta x/c = 10\%$ . Portions of the airfoil are up to 20% of the period, or up to  $\Delta\alpha = 2^\circ$  of the pitching motion, in the intermittent state. The intermittent region is largest at minimum angle of attack and reduces at high angles.

The EDI-M109 shows a large movement of the upper side transition location. The maximum downstream transition position depends on the pitching amplitude and is reached at  $x/c = 50\%$  for the test cases investigated. The maximum upstream position is independent of the model motion at  $x/c = 1\%$ . For attached flow, the temporal transition behaviour is symmetric on the upstroke and the downstroke, whereas the relaminarisation is delayed when separation occurs during dynamic stall. The transition movement is following the model motion with a constant time delay of  $\Delta t/T = 0.02$ . For the flow downstream of  $x/c \approx 5\%$ , a linear relationship could be found between the transition position and the time.

The unsteady transition behaviour revealed a significant hysteresis with respect to the angle of attack. Laminar flow is enhanced during the upstroke and suppressed during the downstroke. The hysteresis increases with the pitching amplitude, both in its streamwise extent and in the

phase lag between the upstroke and the downstroke.

The hot film data also allowed for the analysis of the separation. Dynamic stall was found to be initiated by an abrupt turbulent separation causing leading edge stall during the upstroke. During the downstroke, turbulent reattachment occurs from the leading edge to the trailing edge. No laminar separation was detected, indicating that a laminar separation bubble is not involved in the dynamic stall process on the EDI-M109 airfoil at  $M = 0.3$  and  $Re = 1.8 \times 10^6$ .

## 6. ACKNOWLEDGEMENTS

The authors thank G. Höhler and H.P. Kreplin for sharing their expertise in the field of hot film anemometry. This work was funded by the DLR rotorcraft research programme and the German national LuFo IV research project INROS.

## 7. REFERENCES

- [1] A. Klein, K. Richter, A.R.M. Altmikus, T. Lutz, E. Krämer, "Unsteady criteria for rotor blade airfoil design", 35th European Rotorcraft Forum, Hamburg, 22-25 Sept, 2009.
- [2] S. Schreck, W. Faller and H. Helin, "Pitch Rate and Reynolds Number Effects on Unsteady Boundary Layer Transition and Separation", AIAA94-2256, 25th AIAA Fluid Dynamics Conference, Colorado Springs, CO, 20-23 June, 1994.
- [3] T. Lee and S. Basu, "Measurement of unsteady boundary layer developed on an oscillating airfoil using multiple hot-film sensors", Experiments in Fluids, Vol. 25, pp. 108-117, 1998.
- [4] M.S. Chandrasekhara and M.C. Wilder, "Heatflux gauge studies of compressible dynamic stall", AIAA Journal, Vol. 41, No. 5, pp. 757-762, DOI 10.2514/2.2019, 2003.
- [5] T. Lee and P. Gerontakos, "Investigation of flow over an oscillating airfoil", Journal of Fluid Mechanics, Vol. 512, pp. 313-341, DOI 10.1017/S0022112004009851, 2004.
- [6] P. Lorber and F. Carta, "Unsteady Transition Measurements on a Pitching Three-Dimensional Wing", 5<sup>th</sup> Symposium on Numerical and Physical Aspects of Aerodynamic Flows, Long Beach, CA, January 13-15, 1992.

- [7] K. Richter, A. Le Pape, T. Knopp, M. Costes, V. Gleize and A.D. Gardner, "Improved Two-Dimensional Dynamic Stall Prediction with Structured and Hybrid Numerical Methods", Journal of the American Helicopter Society, Vol. 56, No 4, DOI: 10.4050/JAHS.56.042007, 2011.
  
- [8] A.D. Gardner, K. Richter, H. Mai, A.R.M. Altmikus, A. Klein and C.-H. Rohardt, "Experimental Investigation of Dynamic Stall Performance for the EDI-M109 and EDI-M112 Airfoils", 37th European Rotorcraft Forum, Gallarate, Italy, 13-15 September, 2011.
  
- [9] J. Kiedaisch and M. Acharya, "Investigation of Unsteady Separation over Pitching Airfoils at High Reynolds Numbers", AIAA-98-2975, 29<sup>th</sup> AIAA Fluid Dynamics Conference, Albuquerque, NM, 15-18 June, 1998.
  
- [10] S. Schreck, W. Faller and M. Robinson, "Unsteady Separation Processes and Leading Edge Vortex Precursors: Pitch Rate and Reynolds Number Influences", Journal of Aircraft, Vol. 39, No. 5, pp. 868-875, 2002.